

A diagrammatic description of the equation of motion, current, and noise within the second-order von Neumann approach

O. Karlström¹, C. Emary², P. Zedler², J.N. Pedersen^{1,3}, C. Bergenfeldt¹, P. Samuelsson¹, T. Brandes², A. Wacker¹

¹*Mathematical Physics, University of Lund, Box 118, SE-22100 Lund, Sweden*

²*Institut für Theoretische Physik, Technische Universität Berlin, D-10623 Berlin, Germany*

³*Department of Micro- and Nanotechnology Technical University of Denmark DTU Nanotech, Building 345 East, DK-2800 Kongens Lyngby, Denmark.*

We investigate the second-order von Neumann approach from a diagrammatic point-of-view and demonstrate its equivalence with the resonant tunnelling approximation. Investigation of higher-order diagrams shows that the method correctly reproduces the equation of motion for the single-particle reduced density matrix of an arbitrary non-interacting many-body system. This explains why the method reproduces the current exactly for such systems. We go on to show, however, that diagrams not included in the method are needed to calculate exactly higher cumulants of the charge transport. We analyse the discrepancy between the noise calculated by our method and the exact Levitov formula for a simple non-interacting quantum dot model. Furthermore we study the noise of the canyon of current suppression in a two-level dot, a phenomenon that requires the inclusion of electron-electron interaction as well as higher-order tunneling processes.

PACS numbers: 72.70.+m,73.63.-b,05.60.Gg,73.23.Hk

I. INTRODUCTION

Understanding transport through interacting nanostructures is of major importance for the development of nanoelectronics. The last decades have seen a high activity within the field, but calculating the transport through general interacting systems remains a challenging task. In contrast, transport through non-interacting systems have long-since been well explained by work the of Landauer and Büttiker.¹ In this framework The Full Counting Statistics (FCS) was later developed by Levitov, Lee, and Lesovik.² Lately it was also shown how the exact equations of motion (EOMs) for the reduced density matrix could be derived.^{3,4} In a very recent work it was shown how this could be used for deriving the FCS in the noninteracting limit.⁵ Although very useful in their regime of validity, these methods are restricted to non-interacting systems, and can generally not be applied to study the transport of confined nanostructures, where electron-electron-interactions are of major importance.

To deal with the complications of interacting systems, various methods have been developed. The most widely used technique is the generalized master equation approach which can be derived in many different ways including the real-time diagrammatic technique^{6,7} by Schoeller, König, Schön, and co-workers, as well as the Bloch-Redfield approach originally developed in Refs. 8–10. Comparisons of different approaches have been performed in Refs. 11 and 12. These methods result in a hierarchy of coupled linear differential equations, which must be truncated. Keeping only the lowest non-vanishing order in dot-lead couplings one arrives at first-order methods, valid in the regime where sequential tunneling is dominant. Keeping higher-order terms, methods such as the second order von Neumann (2vN) approach can be derived,¹³ where co-tunneling as well as the coherence between the dot states are included. See also Ref. 14 where

effects of co-tunneling on molecular transport was discussed. Lately Jin et al. developed a method¹⁵ which, at a certain level of approximation was shown to be equivalent to the resonant tunneling approximation within the real-time diagrammatic technique. Equivalence with the 2vN approach was also suggested.

The aim of this paper is to investigate the 2vN approach from a diagrammatic point-of-view. This allows us to establish a number of exact results for the theory. Firstly, we demonstrate the equivalence between the 2vN method and the resonant tunneling approximation, (and thus the method of Jin et al). We then consider non-interacting systems and show that, although the 2vN approach yields the correct EOM for the reduced single-particle density matrix p , enabling an exact calculation of the current,¹⁵ the EOMs for the complete reduced many-body density matrix ρ is not exact. Building on the work of Ref. 16 we consider the 2vN approach with the inclusion of counting fields. Using our diagrammatic method, we are able to explain why the shotnoise calculated for a non-interacting system is not exact, even though the current is. In fact, we find that the inclusion of diagrams of order Γ^4 is required to reproduce the noise correctly (Γ is the lead-dot coupling energy, which contains the square of the tunneling elements¹⁷). Finally, we consider the noise calculated numerically within the 2vN approach for two illustrative models. We compare our noise results for the single-resonant level (SRL) model with the exact results and demonstrate that, despite the limitations discussed above, the 2vN approach still gives a good description of the noise properties of this model for $\Gamma < k_B T$. We then investigate the noise and Fano-factor for the two-level spinless system where a canyon of current suppression was previously observed.^{18,19}

The remainder of the paper is organized as follows: In Sec. II we present the 2vN approach with the inclusion of counting fields¹⁶ and Sec. III gives an overview

of the real-time diagrams employed in this work. The equivalence between the 2vN approach and the resonant tunneling approximation within the real-time diagrammatic technique is discussed at this stage, with details to be found in Appendix B. With these results in place, we first show in Sec. IV that the 2vN approach gives the correct EOM for the reduced density matrix of a single-level system coupled to reservoirs, but that this result does not generalize to the reduced density matrix ρ of a multi-level many-body system. Sections VI and VII contain the results of our 2vN calculations for the single-level system and the interacting two-level system. We then conclude in section VIII.

II. THE SECOND ORDER VON NEUMANN METHOD WITH COUNTING FIELDS

A common transport Hamiltonian describes transitions (T) between two leads via a quantum dot (D) and can be written as

$$\mathcal{H} = \mathcal{H}_{\text{Leads}} + \mathcal{H}_{\text{D}} + \mathcal{H}_{\text{T}}. \quad (1)$$

We assume that the leads are Fermi liquids of electrons with dispersion $E_{k\ell}$. With ℓ we distinguish the different leads. Index k is the (quasi-)momentum quantum number, but it could also contain additional properties like spin:

$$\mathcal{H}_{\text{Leads}} = \sum_{k\ell} E_{k\ell} c_{k\ell}^\dagger c_{k\ell}. \quad (2)$$

We describe the main system, i.e. the quantum dot, in its diagonal basis using the states $|a\rangle$ which can be many-particle states including also bosonic degrees of freedom:

$$\mathcal{H}_{\text{D}} = \sum_a E_a |a\rangle \langle a|. \quad (3)$$

Responsible for transport are tunneling processes between the main system and the leads. These processes are described by terms where the state of the main system changes while at the same time an electron leaves or enters a reservoir. The tunneling Hamiltonian including counting fields is given by²⁰

$$\mathcal{H}_{\text{T}}(\lambda) = \sum_{k\ell, ab} T_{ba}(k\ell) |b\rangle \langle a| c_{k\ell} e^{-i\lambda_\ell/2} + \text{h.c.} \quad (4)$$

In this section we use the convention that dot state $|b\rangle$ contains one more electron than dot state $|a\rangle$, and so on. In this formalism one can derive the generalized Liouville-von-Neumann equation

$$i \frac{d}{dt} \rho(\lambda, t) = \mathcal{H}^+(\lambda) \rho(\lambda, t) - \rho(\lambda, t) \mathcal{H}^-(\lambda), \quad (5)$$

where, like in the rest of the paper, we set $\hbar = 1$ for the sake of simplicity. We have introduced the λ -dependent Hamiltonian

$$\mathcal{H}^\pm(\lambda) = \mathcal{H}_{\text{Leads}} + \mathcal{H}_{\text{D}} + \mathcal{H}_{\text{T}}(\pm\lambda). \quad (6)$$

In Laplace-space Eq. (5) reads

$$iz\hat{\rho}(\lambda, z) = i\rho(\lambda, 0) + \mathcal{H}^+(\lambda)\hat{\rho}(\lambda, z) - \hat{\rho}(\lambda, z)\mathcal{H}^-(\lambda). \quad (7)$$

For states of the whole system we choose a basis of tensor products $|ag\rangle = |a\rangle \otimes |g\rangle$, where $|a\rangle$ describes the complete many particle state of the main system and $|g\rangle$ describes the many particle state of the leads.

We introduce the following quantities

$$\begin{aligned} w_{b'b} &= \sum_g \rho_{b'g;bg}, \\ \phi_{ba}(k\ell) &= \sum_g \rho_{bg-k\ell;ag}, \\ \chi_{ab}(k\ell) &= \sum_g \rho_{ag;bg-k\ell} \end{aligned} \quad (8)$$

where $g - k\ell$ denotes a lead state where an electron with quantum number k in lead ℓ has been removed. Note that $\chi_{ab}(k\ell) \neq \phi_{ba}^*(k\ell)$ due to the inclusion of counting fields. $w_{b'b}$ are the elements of the reduced density matrix. In the EOM these elements couple to ϕ and χ which are the coherences arising from the superpositions of an electron in the leads and the dot. These in turn couple to elements where two electrons are moved between leads and dot. To break this hierarchy of equations the EOM is truncated as described below. This results in a closed EOM which can be solved numerically.

Furthermore we use the following approximations:

- **Factorization:** Wherever an occupation operator of a lead state appears we replace it by a Fermi function, like here:

$$\begin{aligned} \sum_g \langle ag | c_{k\ell}^\dagger c_{k\ell} c_{k'\ell'}^\dagger \hat{\rho}(\lambda, z) | bg \rangle \\ \approx f_{k\ell} \sum_g \langle ag | c_{k'\ell'}^\dagger \hat{\rho}(\lambda, z) | bg \rangle. \end{aligned} \quad (9)$$

- **Truncation:** We neglect all matrix elements where the bra- and the ket-state differ by more than two single-particle states of the leads, like here:

$$\begin{aligned} \langle ag | c_{k_1\ell_1} c_{k_2\ell_2}^\dagger c_{k_3\ell_3} \hat{\rho}(\lambda, z) | bg \rangle \approx 0, \\ \text{if } k_1\ell_1, k_2\ell_2 \text{ and } k_3\ell_3 \text{ are different.} \end{aligned} \quad (10)$$

- **Thermodynamic Limit:** We assume that the set of all states in the leads is uncountable. Hence the occupations on the leads will not change due to the tunneling of single electrons, even not for large times.

Following the derivations in Refs. 13 and 16 we can write down the EOM for ϕ , χ , and w , see Appendix A. Previously implementations of this scheme have solved these equations numerically^{13,16} (and see section VI) but here we are interested in determining analytical properties of the approach. For this purpose the real-time diagrammatic technique^{6,7} is more suitable, as discussed in the following sections.

III. DIAGRAMMATIC DESCRIPTION

In this section we discuss how the EOM for the reduced density matrix of a central quantum system coupled to external leads can be derived using diagrammatic methods.

In deriving the EOM we follow the diagrammatic notation of Ref. 12, where more details on how the diagrams are evaluated can be found. Assuming that total density matrix is a direct product of the initial states of the dot and leads at the time t_0 , when the couplings between leads and dot is switched on, the EOM for the elements of the reduced density matrix $\rho_{b;b'}$ can be written as a closed set of linear equations

$$i\frac{d\rho_{b;b'}}{dt} = -i\sum_{aa'}\delta_{ab}\delta_{a'b'}(E_a - E_{a'})\rho_{a;a'} + \sum_{aa'}\int_{t_0}^t d\tau K_{bb'}^{aa'}(t-\tau)\rho_{a;a'}(\tau), \quad (11)$$

where the first term on the right corresponds to the unitary evolution of the dot not coupled to leads and the second term is generated by tunneling events. Unlike in Sec. II it is not assumed that state $|b\rangle$ contains one more electron than state $|a\rangle$. Here the coefficients $K_{bb'}^{aa'}$ can be calculated using Keldysh diagrams as outlined in Ref. 12. All possible irreducible diagrams connecting the states $|b\rangle$, $|b'\rangle$ on the left with the states $|a\rangle$, $|a'\rangle$ on the right contribute to the coefficient $K_{bb'}^{aa'}$. In an irreducible diagram any vertical cut crosses at least one lead contraction arrow. We use the following notation $|b\rangle = |\alpha, \beta, \dots\rangle$, where anti-symmetrization of the many-particle state is implicitly assumed, to specify which single-particle states $|\alpha\rangle$, $|\beta\rangle, \dots$ that compose the many-body state $|b\rangle$. This way of writing the many-particle state as product states is generally not possible for interacting systems but can always be done in the non-interacting case that we focus on. Here we illustrate how the diagram evaluation works, see Fig. 1, which gives the time evolution on $\rho_{1,2,3;1,2,3}$ in terms of $\rho_{1;1}$. Throughout the paper we use the convention that time increases from right to left. The upper and lower contour gives the time evolution of the bra- and ket-states respectively. This corresponds to different ordering on the contours so that the contour ordering of the tunneling events agrees with the direction of time along the upper branch, while it is opposite to the direction of time on the lower branch. This can be viewed as a Keldysh diagram where time is running backwards along the lower branch.

Here we give a brief summary of the diagrammatic rules of how to evaluate the diagrams. More detailed discussions can be found in Refs. 6, 7, and 12.

1) Each vertex where a lead contraction arrow ends has a related tunneling probability $T_{ba}(kl)$, representing that the dot state changes from many-particle state $|a\rangle$ to many-particle state $|b\rangle$ by the annihilation of an electron in lead-state k in lead l . Arrows pointing out of a branch correspond to Hermitean conjugated processes.

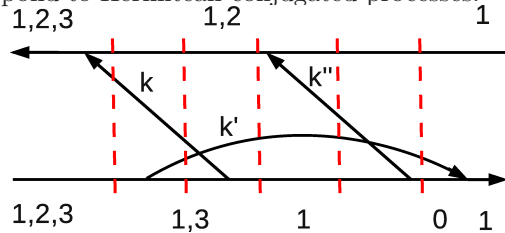


FIG. 1. Example of a 3:rd order diagram included in the 2vN method.

2) In a contraction, the lead operator with the larger time argument comes first unless the right vertex of the contraction is on the lower branch. For Fig. 1 this results in the Fermi factors: $f(E_k)[1 - f(E_{k'})]f(E_{k''})$, where we have included the lead index ℓ in k .

3) The factors in the denominator of the diagram are given by the dashed vertical lines of Fig. 1. Each line gives a factor which is given by (the energy on the lower contour) - (the energy on the upper contour) + (energies of arrows pointing right) - (energies of arrows pointing left). Going from left to right this results in the denominators $E_{1,2,3} - E_{1,2} - E_k$, $E_{1,3} - E_{1,2} - E_k + E_{k'}$, $E_1 - E_{1,2} + E_{k'}$, $E_1 - E_1 + E_{k'} - E_{k''}$, $E_0 - E_1 + E_{k'}$ for Fig. 1. Furthermore $i0^+$ should be added to each factor.

4) The sign of the diagram is given by $(-1)^{N+n_c+n_l} \times$ (Fermion sign), where N is the order of the diagram in Γ , n_c is the number of crossing contraction lines, and n_l is the number of vertices on the lower contour. In Fig. 1 $N = 3$, $n_c = 2$, and $n_l = 4$ so that the first sign factor becomes -1 . Comparing with Ref. 12 the Fermion sign results from the ordering of the dot operators. For the diagram in Fig. 1 the Fermion sign is given by $a_1^\dagger a_1 a_3 a_2 a_3^\dagger a_2^\dagger |1\rangle = -|1\rangle$, i.e. the Fermion sign is negative, resulting in an overall positive sign in front of the diagram.

In total this diagram will contribute to the time evolution of $\rho_{1,2,3;1,2,3}$ in terms of $\rho_{1;1}$ in the following way in the stationary limit, corresponding to $t \rightarrow \infty$ in Eq. 11:

$$i\frac{d}{dt}(\rho_{1,2,3;1,2,3}) = (\text{terms from other diagrams}) + \sum_{k,k',k''} \frac{f(E_k)[1 - f(E_{k'})]f(E_{k''})T_{1,2,3;1,2}(k)T_{1,2,3;1,3}^*(k')T_{1,3;1}^*(k)T_{1,2;1}(k'')T_{1;0}^*(k'')T_{1;0}(k') \times \rho_{1;1}}{(E_{1,2,3} - E_{1,2} - E_k)(E_{1,3} - E_{1,2} - E_k + E_{k'})(E_1 - E_{1,2} + E_{k'})(E_1 - E_1 + E_{k'} - E_{k''})(E_0 - E_1 + E_{k'})}, \quad (12)$$

where spin and lead indices have been included in the k quantum numbers, and the $i0^+$ -terms have been omitted.

The resonant-tunneling approximation was introduced for the SRL in Ref. 21. In diagrammatic terms, this approximation was defined as retaining all irreducible diagrams in the kernel where a vertical cut crosses at most two lead contractions. In Appendix B, we derive an explicit expression for the self-energy implicit to the 2vN approach which shows that the 2vN approach corresponds to exactly this approximation for an arbitrary system. For this purpose the diagrams of the Liouville perturbation theory,²² a variant of the real-time diagrammatic approach, are more appropriate.

IV. CANCELLATION OF DIAGRAMS FOR NON-INTERACTING SYSTEMS

In this Section we show how all diagrams discarded in the resonant tunneling approximation, i.e. the diagrams not included in the 2vN approach, cancel each other in the EOM for the single-particle reduced density matrix in the non-interacting limit. For single level QDs a canceling partner diagram can always be found for each diagram by changing the branch of the second and third leftmost vertices in the diagram, see Figs. 2 and 3. For multi-level QDs the diagrams can be grouped into families, see Fig. 5 where all diagrams have the same absolute value but half contribute to the EOM with plus signs and half with minus signs.

A. Single resonant level

To explain on a diagrammatic basis why the resonant tunneling approximation gives the right EOM for the single-particle reduced density matrix and the right current we consider diagrams with three dot-lead excitations at the same time. We begin by noting that diagrams where different vertices are contracted necessarily have different denominators. When trying to find out how the diagrams cancel a good strategy is therefore to look for diagrams where the same vertices are contracted, i.e. diagrams that correspond to the same Liouvillian diagram (see Appendix B). We will illustrate the canceling using an example diagram seen in Fig. 2. The red numbers on gray backgrounds give the state of the quantum dot, while the black numbers label the vertices. Since it is a single-level quantum dot, we are limited to occupations of $|0\rangle$ or $|1\rangle$. This means that at every second vertex we must create an electron in the dot and in every second we must annihilate an electron. Specifically this means that if we create at vertex 4 we must do the same at vertex 3 if they are on different branches, and if we create at 3 we must annihilate at 4, if they are on the same branch.

A canceling diagram can be found for any third-order diagram not included in the 2vN approach by changing branch of vertex 3 and 4. For Fig. 2 the resulting di-

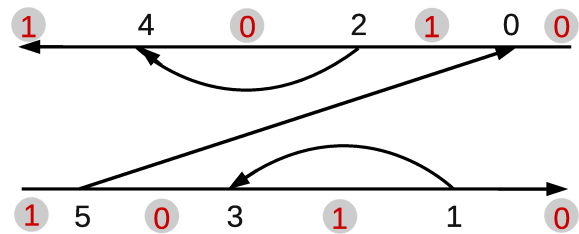


FIG. 2. Example of a 3:rd order diagram, for a single level system, that is not included in the 2vN approach. The red numbers on gray backgrounds denote the dot occupation while the black numbers label the indices.

agram can be seen in Fig. 3. This results in the same change of occupation at the two branches so that the energy denominators are unchanged. As we only moved the left vertices in the contraction, the contributions from the lead contractions (Fermi factors) are also unchanged. Since we are dealing with a single-particle system, we can neglect the Fermion sign and the total sign is given by $(-1)^{N+n_c+n_i}$. Clearly N is unchanged. The change in n_i is 0 or ± 2 , i.e. an even number. The change in n_c is given by the number of dot operators that are commuted. The two moved vertices will both be commuted with the unmoved left vertex 5. Then there is the additional commutation between the two moved vertices. In total n_c is therefore an odd number.

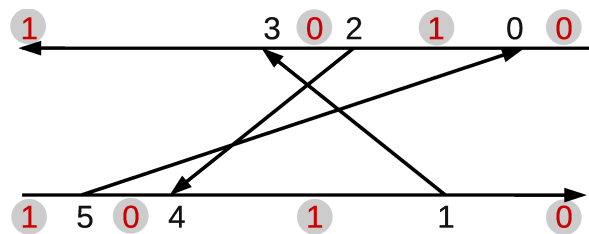


FIG. 3. Canceling partner of diagram in Fig 2.

For higher-order diagrams the reasoning is much the same. A canceling diagram can again be found by moving the second and third leftmost vertices to the other branch. In the same way as for the third-order diagrams the change in number of crossings is an odd number so that the diagrams cancel. This explains on a diagrammatic basis why the 2vN method gives the exact EOM for ρ and the exact current for the single level.¹³

The above described method explains how to cancel diagrams where three dot-lead excitations exist at the same time, i.e. the type of diagrams not included in the 2vN approach. We emphasize that higher order diagrams where the maximum number of dot-lead excitations are restricted to two, see Fig. 4, can not be canceled in this way. Changing branch of the same vertices as before, in Fig. 4 labeled by 2 and 4 since the vertices have been shifted in time, changes the number of crossings in the

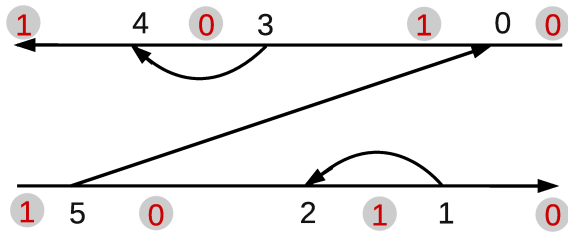


FIG. 4. Example of a higher-order diagram included in the 2vN approach that is not canceled by the above described method.

diagram with an even number. As a result the two diagrams do not cancel. This demonstrates the improvement of the 2vN approach compared to pure second order approaches where diagrams such as Fig. 4 are not included.

B. Canceling of diagrams for multi-level systems

For multiple level QDs there is no requirement that electrons are created/annihilated at every second vertex. Furthermore, in order for the diagrams to cancel the two moved vertices must create/annihilate the same state in the dot. Generally it is not possible to find two such vertices in many-body diagrams. Higher order diagrams can therefore generally not be canceled in the above described way. As a result, the 2vN approach does not give the correct EOM for ρ for many-body systems even in the noninteracting limit. However, we will see that the EOM for the single-particle reduced density matrix

$$p_{\mu;\nu} = \text{Tr}_{\text{dot}} [a_{\nu}^{\dagger} a_{\mu} \rho], \quad (13)$$

where the trace is taken over the dot system, is still correct in this limit. The diagonal states of ρ give the probability of the corresponding many-body state being occupied. This probability corresponds to that exactly the single-particle states that compose the many body state are occupied, the others are empty. The diagonal terms of p give the probability that the corresponding single-particle state is occupied, without considering the occupations of the other single-particle states.

Following the definition of p we have for non-interacting systems

$$p_{\mu;\nu} = \sum_{c: (\mu, \nu \notin c)} \rho_{\mu+c; \nu+c} \quad (14)$$

Here, the state $\mu + c$ is the many-particle state c with a particle added in single-particle state μ . To get the time evolution of $p_{\mu;\nu}$ in terms of $\rho_{a;a'}$ we must therefore sum over all diagrams giving the time evolution of $\rho_{\mu+c; \nu+c}$ in terms of $\rho_{a;a'}$. In this sum many of the diagrams will have the same energy denominators and Fermi factors, i.e. the values of the diagrams are equal, which means that they cancel if they have opposite sign. We will see that a

family of diagrams can be constructed by starting from a diagram such as the one in Fig. 5a), and then change branch of the left vertices where the single-particle states composing $|c\rangle$ are created. The family that the diagram in Fig. 5a) belongs to is shown in Fig. 5. It should be noted that the energy denominators of the different diagrams in a family are only equal in the non-interacting limit. For interacting systems the diagrams do not cancel.

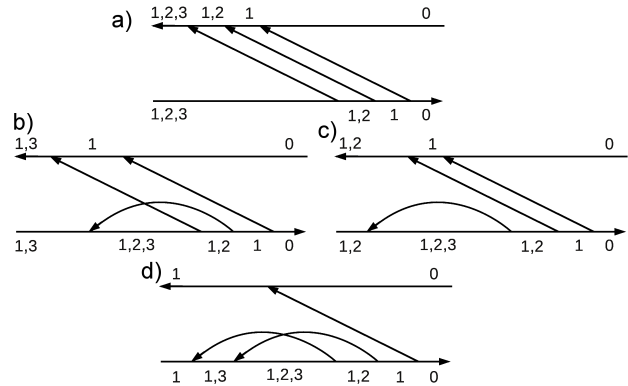


FIG. 5. A family of canceling diagrams.

All states on the left contain single-particle state μ . In Fig. 5 we see that we have $|\mu\rangle = |1\rangle$, and on the right we have the state $|0\rangle$. This family of diagrams thus contribute to the time evolution of $p_{1;1}$ in terms of $\rho_{0;0}$. Starting from the state on the left side, the energy denominators tell us if we should add/remove states on the upper/lower branch. This determines how the dot states should be created and annihilated on the upper and lower branch at the N left vertices. This determines the direction of the contraction arrows. Thus, having chosen the states $|b\rangle$ and $|b'\rangle$ on left side of the diagram, there is only one possibility for the N right vertices if we restrict to diagrams where the same vertices are contracted, i.e. diagrams which correspond to the same Liouvillian diagram (see Appendix B-F). We denote the number of vertices at the upper branch, where single-particle states composing $|c\rangle$ are created or annihilated, by k . Denoting the maximum number of single-particle states in $|c\rangle$ by n , $n = 2$ in Fig. 5 corresponding to the states $|2\rangle$ and $|3\rangle$, the number of diagrams with k vertices on the upper branch is given by $\binom{n}{k}$. We first show that all diagrams with a given k have the same sign. In the expression $(-1)^{N+n_c+n_l}$ the number of crossings between contraction lines changes when we move one vertex from the upper to the lower and one from the lower to the upper, see Fig. 5 b) and c). However, this is canceled by the additional change in the Fermion sign, as each change in the number of crossings is related to the commutation of two Fermion operators of different dot states. In total there will therefore not be a sign change, i.e. diagrams such as Fig. 5 b) and c) have the same sign. Next we show that the sign changes when k is changed by one. Moving a

vertex can result in a change in the number of crossing contraction lines, but this number is again the same as the number of fermion operators that is commuted due to the change. Left is only the change in sign due to that the number of vertices on the lower branch has changed by one. In the general case one therefore gets a sum

$$\sum_{k=0}^n (-1)^k \binom{n}{k} = 0 \quad \text{for } n \geq 1. \quad (15)$$

Since each diagram belongs to one and only one family and each family gives no contribution we conclude that the diagrams give no contribution if $n \geq 1$.

We now have to show that higher-order diagrams, with $N \geq 3$, always have $n \geq 1$. If $n = 0$ this means that the states b and b' on the left side of the diagram are single-particle states, and no other states can be created/annihilated in the diagram. This also means that a and a' do not contain any single-particle states other than b and b' . Now there are two possibilities: 1) $b = b'$, this case is exactly the single-particle case described in Sec. III. 2) $b \neq b'$, for $N \geq 3$, at least two of the N vertices to the left must act on the same state. These two vertices must necessarily be on the same branch and one creates the state while the other annihilates the state. If there is no creation vertex of the same state on the other branch to the left of these two vertices, a canceling diagram is found by changing branch of the two vertices, see Fig. 6 a). In the other case one changes branch on the two creation vertices, see Fig. 6 b). Thus the higher-order diagrams for the time evolution of the coherence between single-particle states can be canceled by the same method we used when canceling diagrams for the single level dot. This canceling of diagrams works for all diagrams not included in the 2vN approach to the best of our knowledge.

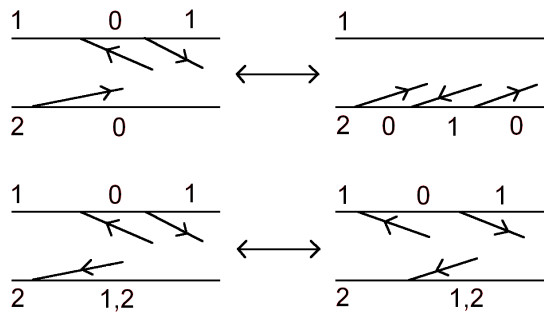


FIG. 6. Example of many-body diagrams that cancel directly for ρ . The red numbers indicate which states of the dot that are filled.

To conclude one can divide all diagrams into those that cancel directly for ρ , and those that cancel only for p . The ones that cancel directly for ρ can be canceled by moving two vertices in a way that does not change b and b' . To cancel the rest of the diagrams for p the diagrams are divided into families. All diagrams within a family contributes to the time evolution of the same element in

p . All diagrams in the family have the same value but half contribute with a plus sign and half with a minus sign. As a result of the exact EOM for p , the current can be calculated exactly for any non-interacting system, as outlined in Ref. 15.

It is interesting to note that although the 2vN method does not correctly reproduce ρ , it can in some cases still be calculated exactly using the knowledge that the EOM for p is exact. For systems where the probability to tunnel into superpositions of the dot states can be neglected, such as the non-interacting Anderson model or dots where the level spacing greatly exceeds the coupling strengths so that the secular approximation can be performed, each dot level can be treated independently from the others. This allows us to write down the following expression for the diagonal elements of ρ ,

$$\rho_{b;b} = \prod_{\alpha \in b} p_{\alpha;\alpha} \prod_{\beta \notin b} (1 - p_{\beta;\beta}), \quad (16)$$

where the first product is over all single-particle states composing b and the second product is over those not belonging to b . For such systems the 2vN method thus allows for an exact derivation of the EOM also for ρ .

V. CALCULATING THE NOISE FOR SINGLE RESONANT LEVEL SYSTEMS

The time-evolution propagator can be defined according to

$$\rho(t) = \Pi(t, t_0) \rho(t_0) \quad (17)$$

From the above discussion it is evident that $\Pi(t, t_0)$ is correctly reproduced by the 2vN approach for single-particle systems. The Fourier transform defines $\Pi(\omega)$. Following Ref. 23 we furthermore define $J_{1a}(\omega)$ and $J_{1b}(\omega)$. The diagrams contributing to $J_{1a}(\omega)$ and $J_{1b}(\omega)$ are equivalent to those contributing to the self energy $\Sigma(\omega)$ except that one tunneling vertex has been replaced by a current vertex. In $J_{1a}(\omega)$ the leftmost vertex have been replaced, while in $J_{1b}(\omega)$ any replacement is possible. Such a replacement changes the value of a diagram by a factor of 1/2 and furthermore introduces a sign change if the current vertex is moved to the other branch. We also define $J_{2a}(\omega)$ where two tunneling vertices have been replaced by current vertices. One of the current vertices must be to the left, the other can be at any position.

The noise can then be calculated as

$$S(\omega) = \frac{e^2}{2} \text{Tr}_{\text{dot}} [J_{2a}(\omega) \rho_{st} + J_{1a}(\omega) \Pi(\omega) J_{1b}(\omega) \rho_{st}] - 2\pi \delta(\omega) \langle I \rangle^2 + \text{terms with } (\omega \rightarrow -\omega), \quad (18)$$

where ρ_{st} is the stationary solution to the reduced density matrix. The reason that J_{1a} and J_{2a} needs a current vertex at the leftmost position is that when the trace is taken and the Keldysh contour closed all diagrams with

a tunneling vertex to the left will cancel each other. This results from the sign due to the change in n_l , see Ref. 23 and the references therein.

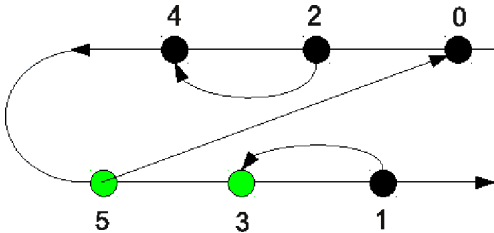


FIG. 7. Example of a 3:rd order noise diagram for J_{2a} that can not be canceled by the above described method. The green dots correspond to current vertices while the black represent normal tunneling vertices. The trace in Eq. 18 is represented by the closing of the Keldysh contour.

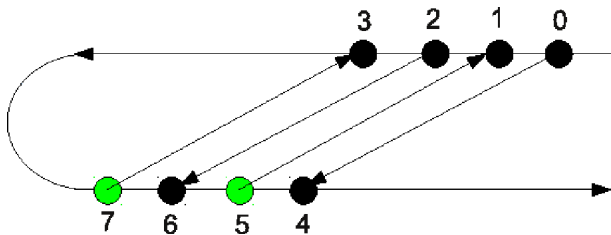


FIG. 8. Example of a 4:th order noise diagram for J_{2a} that can not be canceled by the above described method. The green dots correspond to current vertices while the black represent normal tunneling vertices. The trace in Eq. 18 is represented by the closing of the Keldysh contour.

The diagrams in the J_{1a} block excluded from the 2vN scheme can be canceled by the same method as described above where the leftmost tunneling vertex is not moved. However, the current vertex in blocks J_{1b} and J_{2a} that occurs at positions other than leftmost prevents the canceling of diagrams. Replacing tunneling vertex 3 in Fig. 2 by a current vertex results in the diagram of Fig. 7. This diagram can not be canceled as moving vertex 3 and 4 now results in an additional sign change due to the current vertex. Thus, this 3:rd order diagram is likely to

contribute to the noise.

There are also 4:th order diagrams that contribute to the shot noise, see Fig. 8.

Going to fifth order or higher, one can always find two normal tunnel vertices that can be moved without resulting in a diagram with double occupation. 4:th order in Γ is thus required to calculate the shot noise exactly for the single level. Each order of cumulants in the FCS adds an additional current vertex, see Appendix B. As a result one needs to include two more orders of diagrams, which quickly results in great numerical efforts being required.

It should be pointed out that we have not presented a proof that the 3:rd and 4:th order noise diagrams do not cancel. Rather we have shown that the method by which the diagrams for the EOM cancel, does not work for the noise diagrams. It could be argued that the noise diagrams cancel by some other manner, but previous numerical work have shown that the 2vN method does not reproduce the noise exactly for the single resonant level.¹⁶ That 4:th order diagrams are required is also expected from the Levitov formula. In the low-temperature limit the noise is proportional to $T(1-T)$, T being the transmission function. Here the T^2 term is proportional to Γ^4 . It is interesting to note that although the 2vN approach does not give the correct noise, it can still be obtained by inserting the correct transmission function from the 2vN method into the Levitov formula. In the non-interacting limit the transmission function can be obtained from the current as it does not depend on the applied voltage.

VI. THE SINGLE RESONANT LEVEL

Having seen that higher-order terms are required to correctly reproduce the noise of single-particle systems it is of interest to see how large the discrepancy is between the 2vN method and the exact results using the Levitov formula.

To get an impression of this discrepancy, we apply the 2vN approximation to the noise in the single resonant level model.

Assuming the (constant) tunneling rates $\Gamma_\alpha = 2\pi \sum_k |t_{k\alpha}|^2 \delta(E - E_{k\alpha})$ and $\Gamma = \Gamma_L + \Gamma_R$, and defining the quantity $B_\alpha(E) \equiv 2\pi \sum_k t_{k\alpha}^* \phi_{10}(z, \lambda; k\alpha) \delta(E - E_{k\alpha})$, we obtain the EOM for the single resonant level

$$\begin{aligned}
izw_{00}(z, \lambda) - iw_{00}(t=0, \lambda) &= \sum_{\alpha} e^{i\lambda_{\alpha}/2} \int \frac{dE}{2\pi} [B_{\alpha}(E) - \bar{B}_{\alpha}(E)], \\
izw_{11}(z, \lambda) - iw_{11}(t=0, \lambda) &= - \sum_{\alpha} e^{-i\lambda_{\alpha}/2} \int \frac{dE}{2\pi} [B_{\alpha}(E) - \bar{B}_{\alpha}(E)], \\
\left(E - E_d + iz - \Gamma \int \frac{dE'}{2\pi} \frac{1}{E - E' + iz} \right) B_{\alpha}(E) &= e^{-i\lambda_{\alpha}/2} f_{\alpha}(E) \Gamma_{\alpha} \left(w_{00}(z, \lambda) + \sum_{\alpha'} e^{i\lambda_{\alpha'}/2} \int \frac{dE'}{2\pi} \frac{\bar{B}_{\alpha'}(E')}{E' - E - iz} \right) \\
&\quad - e^{i\lambda_{\alpha}/2} [1 - f_{\alpha}(E)] \Gamma_{\alpha} \left(w_{11}(z, \lambda) - \sum_{\alpha'} e^{-i\lambda_{\alpha'}/2} \int \frac{dE'}{2\pi} \frac{\bar{B}_{\alpha'}(E')}{E' - E - iz} \right).
\end{aligned} \tag{19}$$

These equations have simple analytical solutions at infinite bias, when the tunneling rates are constant or have a Lorentzian shape.¹⁶ At finite bias however, we need a numerical solution and hence must transform the function $B(E)$ into a mapping on a discrete and finite set. Two numerical solution procedures (A and B) have been independently developed.

- **A Discrete energies:** In our first approach¹³ we choose a set of equidistant energies and approximate the integrals with sums over these energies. This requires a cutoff at some energy and is therefore most efficient for scenarios where a sufficiently small energy interval determines the transport properties.
- **B Cutoff in residues:** One can show that in the crucial complex half plane the quantity $B(E)$ has the same poles as the Fermi function.²⁴ By this knowledge the integrals can be approximated with the residues that are closest to the real axis. This leads to an inaccuracy in the value of the Fermi functions. Thus, this method is most efficient when the transport happens at energies where the left and the right Fermi function differ sufficiently.

The two methods also differed in the way the noise was evaluated:

- **A Numerical time evolution:** We evaluate the time evolution of the cumulant generating function $S(\lambda, t) = -\ln[\sum_b w_{bb}(\lambda, t)]$. After a short time, $S(\lambda, t)$ becomes linear in time and its slope can be identified as the noise.
- **B Long time expansion in Laplace space:** By comparing the factors in front of the system states w_{ab} in Eq. (19) we can extract a non-Markovian master equation. As soon as this is known, we can use a Taylor expansion around $z = 0$ and the techniques described in Ref. 25 to calculate the noise.

In approach A the EOM is solved in time space by performing the Markov approximation for the density matrix elements containing two dot-lead excitations. In Laplace space this corresponds to replacing all z to the right of

the equality sign in Eq. (A2) with positive infinitesimals while keeping the other z in the EOM. Using somewhat hand-waving arguments it is easy to realize that doing the Markov approximation at a higher-order is less of an approximation. The z to the right of the equality sign in Eq. (A2) contribute when the rest of the denominator is small. This region can be defined as a volume in the N -dimensional energy space, N being the order at which the Markov approximation is done. As N increases this volume becomes smaller compared to the entire integration volume, which reduces the effect of neglecting the z .

The accuracy of the 2vN approach and the effect of the partial Markovian approximation is investigated in Fig. 9 where the noise, i.e. the second cumulant $\langle\langle I^2 \rangle\rangle$, is shown as a function of the bias, V_{bias} , for two different coupling strengths. The dot level is positioned in the middle of the bias window and we assume equal couplings to left and right lead, $\Gamma_L = \Gamma_R$. Partial Markovian results from approach A are compared with the non-Markovian results of approach B, and the exact non-interacting results of the Levitov formula. For both coupling strengths it can be seen that the effect of performing the partial Markov approximation as described above, is very small. Partial Markovian calculations were also performed using approach B. This gave results indistinguishable from approach A. For weak couplings such as Fig. 9 a) the 2vN results agree well with the exact transmission results as higher-order terms are of less importance (note the y-axis scale). For the stronger couplings of Fig. 9 b) the agreement is good in the low bias limit. As the bias is increased the phase space for higher-order processes increases which causes a discrepancy between the two methods.

VII. NOISE AND FANO FACTOR FOR THE CANYON OF CURRENT SUPPRESSION

So far the success and shortcoming of the 2vN method have been studied. In this section we change focus and use the partial Markovian version A of the method to calculate the noise and Fano factor of the canyon of current suppression, previously investigated

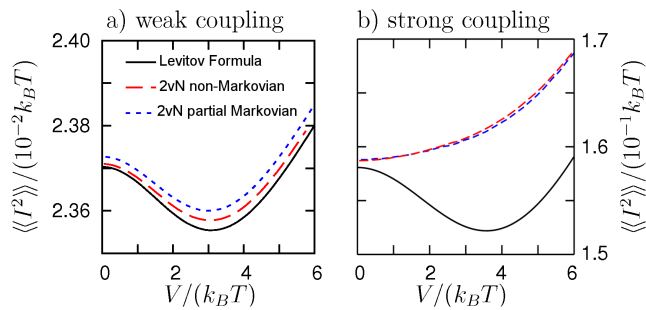


FIG. 9. The noise $\langle\langle I^2 \rangle\rangle$ for a single-level model for a) $\Gamma_L = \Gamma_R = 0.1k_B T$, b) $\Gamma_L = \Gamma_R = k_B T$, and the dot level positioned at the middle of the bias window.

experimentally¹⁸ and theoretically.^{19,26–30} The canyon appears as a suppression of current in both sequential and co-tunneling regimes, close to degeneracy in two-level spinless systems. Noise calculations for this system have previously been performed in Ref. 31 under the assumption that one level was very weakly coupled to the reservoirs.

We parametrize the energy levels as

$$E_{1/2} = \pm \frac{\Delta E}{2} - E_g - U/2, \quad (20)$$

where ΔE is the splitting between the two levels, E_g is a common shift of the levels experimentally achieved by a back gate, and U is the charging energy of the dot due to Coulomb interaction between the two levels.

Figures 10a)-c) show normalized current $\langle\langle I \rangle\rangle / V_{\text{bias}}$, normalized noise $\langle\langle I^2 \rangle\rangle / V_{\text{bias}}$, and the Fano factor $F = \langle\langle I^2 \rangle\rangle / \langle\langle I \rangle\rangle$ as a function of V_{bias} and E_g using the parameters $V_{\text{bias}} = 15k_B T$, $\Gamma_{L1} = \Gamma_{R1} = 4k_B T$, $\Gamma_{L2} = \Gamma_{R2} = k_B T$, and $U = 25k_B T$ corresponding to the parameters of Fig. 2(g) in Ref. 19. A canyon is visible for both the current and the noise, while the Fano factor exhibits a "ridge" close to degeneracy ($\Delta E = 0$). Close to particle-hole symmetry ($E_g = 0$) the ridge is weak, $F \approx 1$. Here the dot is always filled with one electron and the current is carried by the co-tunneling processes described by Eq. (18) of Ref. 19. The conductivity of the system does not depend on which state the system is in and therefore the tunneling events are uncorrelated and $F \approx 1$. As E_g is changed the conductance depends on whether the weakly or strongly coupled level is filled. As a result F increases. This increase can also be due to the onset of thermal noise as the levels move closer to the bias window.

Furthermore, the Fano factor has two "hills" located at $\Delta E/k_B T = -10$, $E_g/k_B T = 5$ and $\Delta E/k_B T = 10$, $E_g/k_B T = -5$. These hills result from the trapping in a low conducting state. The level configuration at $\Delta E/k_B T = 10$, $E_g/k_B T = -5$, marked by a white cross in Fig. 10 b), is shown in Fig. 10 d). The normal state of the dot is $|2\rangle$ being filled, which corresponds to a very low conductance, as current is carried by co-tunneling

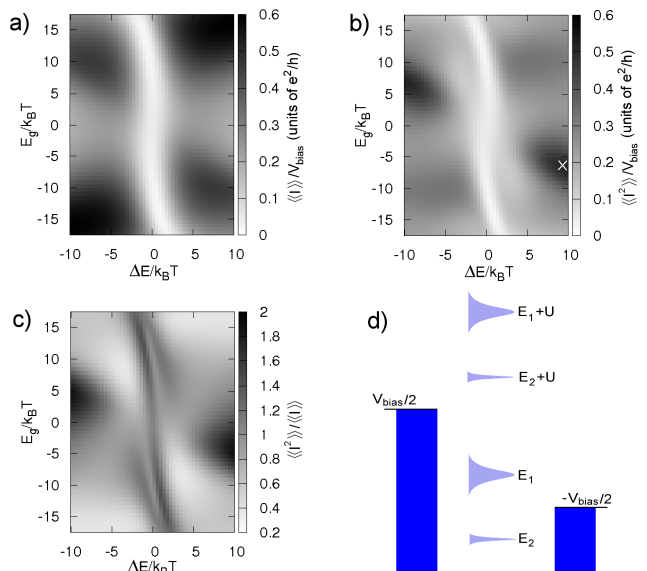


FIG. 10. a) The normalized current $\langle\langle I \rangle\rangle / V_{\text{bias}}$, b) the normalized noise $\langle\langle I^2 \rangle\rangle / V_{\text{bias}}$, in units of e^2/h , and c) the Fano factor $F = \langle\langle I^2 \rangle\rangle / \langle\langle I \rangle\rangle$. The parameters are given by $V_{\text{bias}} = 15k_B T$, $\Gamma_{L1} = \Gamma_{R1} = 4k_B T$, $\Gamma_{L2} = \Gamma_{R2} = k_B T$, and $U = 25k_B T$. d) The level positions at the white cross of b).

processes through either the weakly coupled state $|2\rangle$ or through state $|1\rangle$ which is far from the bias window due to Coulomb interaction. However, sometimes inelastic co-tunneling events empty $|2\rangle$ and fill $|1\rangle$, resulting in a highly conductive system. As a result the electron transport is bunched which corresponds to a large noise signal and a high Fano factor.

VIII. CONCLUSIONS

The 2vN method and the resonant tunneling approximation within the real-time diagrammatic approach were compared using Liouvillian perturbation theory. This established the equivalence between the two methods and the recently developed method of Ref. 15. Using diagrammatic techniques it was shown how diagrams of third and higher order in the lead-dot coupling energy canceled in the EOM for the single-particle reduced density matrix of non-interacting systems. This enables the exact calculation of the current. However, it was seen that to correctly reproduce the EOM for the many-body density matrix, or the Full Counting Statistics, diagrams of higher-order were needed. The discrepancy in the noise between the 2vN method and the exact Levitov formula was investigated in the non-interacting limit. For stronger lead-dot couplings an increased discrepancy was observed at larger bias, due to an increased phase space for higher-order tunneling. Finally, the noise of the canyon of current suppression was calculated using

the 2vN method. While the current and noise showed a canyon around level degeneracy, the Fano factor exhibited a ridge, as well as local maxima due to electron bunching.

and project BR 1528/8. We are grateful to Martin Leijnse and Tomas Novotny for useful discussions.

ACKNOWLEDGMENTS

This work was supported by the Swedish research council and Deutsche Forschungsgesellschaft via SFB 910

Appendix A: Equation of motion for the 2vN approach including counting fields

The EOM is given by

$$(z - E_b + E_{b'})w_{bb'} = + \sum_{a,k\ell} e^{i\lambda\ell/2} (T_{ba}(k\ell)\chi_{ab'}(k\ell) - \phi_{ba}(k\ell)T_{b'a}^*(k\ell)) \\ + \sum_{c,k\ell} e^{-i\lambda\ell/2} (T_{cb}^*(k\ell)\phi_{cb'}(k\ell) - \chi_{bc}(k\ell)T_{cb'}(k\ell)) \quad (\text{A1})$$

$$(z - E_c + E_b + E_k)\phi_{cb}(k\ell) = \\ + \sum_{b'} e^{i\lambda\ell/2} T_{cb'}(k\ell)f_{k\ell}w_{b'b} - \sum_{c'} (1 - f_{k\ell})w_{cc'}T_{c'b}(k\ell) e^{-i\lambda\ell/2} \\ + \sum_{a,b',k'\ell'} \frac{[e^{i\lambda\ell'} T_{cb'}(k'\ell')f_{k'\ell'}\phi_{b'a}(k\ell) - (1 - f_{k\ell})\phi_{cb'}(k'\ell')T_{b'a}(k\ell)e^{i(\lambda\ell' - \lambda\ell)/2}] T_{ba}^*(k'\ell')}{E_k + E_{k'} - (E_c - E_a) + z} \\ + \sum_{a,b',k'\ell'} \frac{[(1 - f_{k'\ell'})\phi_{cb'}(k\ell)T_{b'a}(k'\ell') - e^{i(\lambda\ell' + \lambda\ell)/2} T_{cb'}(k\ell)f_{k\ell}\phi_{b'a}(k'\ell')] T_{ba}^*(k'\ell')}{E_k + E_{k'} - (E_c - E_a) + z} \\ + \sum_{a,b',k'\ell'} \frac{T_{cb'}(k'\ell') [f_{k'\ell'}\phi_{b'a}(k\ell)T_{ba}^*(k'\ell')e^{i\lambda\ell'} - e^{i(\lambda\ell' + \lambda\ell)/2} T_{b'a}(k\ell)f_{k\ell}\chi_{ab}(k'\ell')]}{E_k - E_{k'} - (E_{b'} - E_b) + z} \\ + \sum_{b',c',k'\ell'} \frac{T_{cb'}(k'\ell') [T_{c'b'}^*(k'\ell')(1 - f_{k'\ell'})\phi_{c'b}(k\ell) - (1 - f_{k\ell})\chi_{b'c'}(k'\ell')T_{c'b}(k\ell)e^{i(\lambda\ell' - \lambda\ell)/2}]}{E_k - E_{k'} - (E_{b'} - E_b) + z} \\ + \sum_{b',c',k'\ell'} \frac{[f_{k'\ell'}\phi_{cb'}(k\ell)T_{c'b'}^*(k'\ell') - e^{i(\lambda\ell' - \lambda\ell)/2} T_{cb'}(k\ell)f_{k\ell}\chi_{b'c'}(k'\ell')] T_{c'b}(k'\ell')}{E_k - E_{k'} - (E_c - E_{c'}) + z} \\ + \sum_{c',d,k'\ell'} \frac{[e^{-i\lambda\ell'} T_{dc}^*(k'\ell')(1 - f_{k'\ell'})\phi_{dc'}(k\ell) - (1 - f_{k\ell})\chi_{cd}(k'\ell')T_{dc'}(k\ell) e^{-i(\lambda\ell' + \lambda\ell)/2}] T_{c'b}(k'\ell')}{E_k - E_{k'} - (E_c - E_{c'}) + z} \\ + \sum_{c',d,k'\ell'} \frac{T_{dc}^*(k'\ell') [(1 - f_{k'\ell'})\phi_{dc'}(k\ell)T_{c'b}(k'\ell') e^{-i\lambda\ell'} - e^{i(\lambda\ell' - \lambda\ell)/2} T_{dc'}(k\ell)f_{k\ell}\phi_{c'b}(k'\ell')]}{E_k + E_{k'} - (E_d - E_b) + z} \\ + \sum_{c',d,k'\ell'} \frac{T_{dc}^*(k'\ell') [T_{dc'}(k'\ell')f_{k'\ell'}\phi_{c'b}(k\ell) - (1 - f_{k\ell})\phi_{dc'}(k'\ell')T_{c'b}(k\ell)e^{-i(\lambda\ell' + \lambda\ell)/2}]}{E_k + E_{k'} - (E_d - E_b) + z}, \quad (\text{A2})$$

The EOM for χ can be obtained by taking the complex conjugate of Eq. A2 followed by replacing λ with $-\lambda$, ϕ_{ba}^* with χ_{ab} , and χ_{ab}^* with ϕ_{ba} . It should be noted that ϕ , χ , and w all depend on the counting fields λ_ℓ .

Appendix B: The 2vN method in Liouville space

The structure of the 2vN scheme can nicely be seen using the diagrams of Liouvillian perturbation theory.^{32,33} We will first discuss the theory without counting field, and include it at the end.

1. Liouville space

The von Neumann equation for the evolution of the total density matrix under Hamiltonian Eq. (1) reads:

$$\dot{\rho}(t) = -i[\mathcal{H}, \rho(t)] = \mathcal{L}\rho(t). \quad (\text{B1})$$

which defines the Liouvillian super-operator \mathcal{L} . In accordance with the decomposition of the Hamiltonian, \mathcal{L} consists of three parts: $\mathcal{L} = \mathcal{L}_{\text{res}} + \mathcal{L}_{\text{D}} + \mathcal{L}_{\text{T}}$ with $\mathcal{L}_{\text{res}} = -i[\mathcal{H}_{\text{Leads}}, \bullet]$, $\mathcal{L}_{\text{D}} = -i[\mathcal{H}_{\text{D}}, \bullet]$, and $\mathcal{L}_{\text{T}} = -i[\mathcal{H}_{\text{T}}, \bullet]$. To ease book-keeping, we introduce a compact single index “1” to denote the triplet of indices (ξ_1, k_1, l_1) . The first index $\xi_1 = \pm$ describes whether a reservoir operator is a creation or annihilation operator:

$$a_1 = a_{\xi_1 k_1 l_1} = \begin{cases} c_{k_1 l_1}^\dagger, & \xi_1 = + \\ c_{k_1 l_1}, & \xi_1 = - \end{cases}. \quad (\text{B2})$$

Similarly we define

$$g_1 = \begin{cases} \sum_{ab} T_{ab}^*(kl) |a\rangle\langle b|, & \xi_1 = + \\ \sum_{ab} T_{ab}(kl) |b\rangle\langle a|, & \xi_1 = - \end{cases}, \quad (\text{B3})$$

such that the tunnel Hamiltonian can be written $\mathcal{H}_{\text{T}} = \xi_1 a_1 g_1$, with all summations left implicit. The notation $\bar{1}$ refers to the triple $(-\xi_1, k_1, l_1)$.

The tunnel Liouvillian $\mathcal{L}_{\text{T}} = -i[\xi_1 a_1 g_1, \bullet]$ consists of system and bath operators acting from both the left and the right. i.e. on both Keldysh branches. We introduce the superscript Keldysh index $p = \pm$ to describe these two possibilities and define corresponding superoperators in Liouville space. For the reservoir, we define \mathcal{L} -space superoperator A via its action on density operator ρ :

$$A_1^p |\rho\rangle\rangle \leftrightarrow \begin{cases} a_1 \rho, & p = + \\ \rho a_1, & p = - \end{cases}. \quad (\text{B4})$$

Following Ref. 33, we define the system superoperators

$$M_f(1, 4) = -p_3 f(-\xi_3 p_3 \omega_3) \left(\delta_{14} G_3^{p_2} \frac{1}{z - x_3 - x_1 - \mathcal{L}_{\text{D}}} \tilde{G}_3^{p_3} - \delta_{13} \delta_{42} G_4^{p_2} \frac{1}{z - x_4 - x_1 - \mathcal{L}_{\text{D}}} \tilde{G}_1^{p_3} \right), \quad (\text{B9})$$

where $x_1 = -i\xi_1(\omega_1 + \mu_1)$ with ω_1 the energy of lead mode (k_1, l_1) and μ_1 the chemical potential of lead l_1 .

3. The 2vN self-energy

An expression for the system self-energy within the 2vN method can be derived by iterating Eq. (B8). Defining the free system propagator $\Omega(1) = [z - x_1 - \mathcal{L}_{\text{D}}]^{-1}$ we obtain

$$\begin{aligned} |\phi(1)\rangle\rangle &= \Omega(1) \left\{ T_f(1) |w\rangle\rangle + \sum_2 M_f(1, 2) |\phi(2)\rangle\rangle \right\} \\ &= \Omega(1) T_f(1) |w\rangle\rangle + \Omega(1) \sum_2 M_f(1, 2) \left\{ \Omega(2) T_f(2) |w\rangle\rangle + \Omega(2) \sum_3 M_f(2, 3) |\phi(3)\rangle\rangle \right\} \\ &= \Omega(1) T_f(1) |w\rangle\rangle + \Omega(1) M_f(1, 2) \Omega(2) T_f(2) |w\rangle\rangle + \Omega(1) M_f(1, 2) \Omega(2) M_f(2, 3) \Omega(2) T_f(3) |w\rangle\rangle + \dots \end{aligned} \quad (\text{B10})$$

Substituting into Eq. (B8) and solving gives

$$|w(z)\rangle\rangle = \frac{1}{z - \mathcal{L}_{\text{D}} - \Sigma(z)} |w(t_0)\rangle\rangle \quad (\text{B11})$$

G via

$$G_1^p O = \sigma^p \times \begin{cases} g_1 O, & p = + \\ -O g_1, & p = - \end{cases}. \quad (\text{B5})$$

The object σ^p is a dot-space superoperator with matrix elements

$$(\sigma^p)_{ss', \bar{s}\bar{s}'} = \delta_{s\bar{s}} \delta_{s'\bar{s}'} \begin{cases} 1, & N_s - N_{s'} = \text{even} \\ p, & N_s - N_{s'} = \text{odd} \end{cases}, \quad (\text{B6})$$

where, N_s is the number of electrons in state s . The tunnel Liouvillian can then be written

$$\mathcal{L}_{\text{T}} = -i\xi_1 p \sigma^p A_1^p G_1^p. \quad (\text{B7})$$

2. The 2vN EOMs in Liouville space

Arranging the elements $w_{b' b}$ into the vector $|w\rangle\rangle$ and elements $\phi_{ba}(k_1 l_1)$ into vector $|\phi(1)\rangle\rangle$ the 2vN EOMs (without counting field), Eq. (A1) and Eq. (A2), read in Liouville space

$$\begin{aligned} z |w\rangle\rangle - |w\rangle\rangle(t_0) &= \mathcal{L}_{\text{D}} |w\rangle\rangle + \sum_1 T(1) |\phi(1)\rangle\rangle \\ z |\phi(1)\rangle\rangle &= (x_1 + \mathcal{L}_{\text{D}}) |\phi(1)\rangle\rangle + T_f(1) |w\rangle\rangle \\ &\quad + \sum_4 M_f(1, 4) \phi(4) \end{aligned} \quad (\text{B8})$$

with $T(1) = i\tilde{G}_1^{p_2}$, with the tilde reminding us that the superoperator G acquires an internal factor p_2 from its constituent σ superoperator as it acts on an odd-charge-coherence state, and $T_f(1) = ip_2 f(-\xi_1 p_2 \omega_1) G_1^{p_2}$ with Fermi function $f(\omega) = [e^{\beta\omega} + 1]^{-1}$, and finally

with the (nonMarkovian) self-energy

$$\Sigma(z) = T(1)\Omega(1)T_f(1) + T(1)\Omega(1)M_f(1,2)\Omega(2)T_f(2) + T(1)\Omega(1)M_f(1,2)\Omega(2)M_f(2,3)\Omega(3)T_f(3) + \dots \quad (\text{B12})$$

with summation over all indices is implied.

This we can write in a compact form. Let \mathbf{T} be a vector with elements $T(1)$, \mathbf{T}_f be a vector with elements $T_f(1)$. Furthermore let \mathbf{M} be the matrix with elements $M_f(1,2)$ and finally, $\mathbf{\Omega}$ be a diagonal matrix with elements $\Omega(1)\delta_{1,2}$. The self-energy can then be written

$$\Sigma(z) = \mathbf{T} \cdot \mathbf{\Omega} \cdot \mathbf{T}_f + \mathbf{T} \cdot \mathbf{\Omega} \cdot \mathbf{M} \cdot \mathbf{\Omega} \cdot \mathbf{T}_f + \mathbf{T} \cdot \mathbf{\Omega} \cdot \mathbf{M} \cdot \mathbf{\Omega} \cdot \mathbf{M} \cdot \mathbf{\Omega} \cdot \mathbf{T}_f + \dots, \quad (\text{B13})$$

which can clearly be resummed to give

$$\Sigma(z) = \mathbf{T} \cdot \frac{1}{1 - \mathbf{\Omega} \cdot \mathbf{M}} \cdot \mathbf{\Omega} \cdot \mathbf{T}_f \quad (\text{B14})$$

which is a very nice clean result.

This self-energy can be expanded in terms of the diagrams of Liouville perturbation theory, see Refs. 22, 32, and 34. Writing out all diagrams up to sixth order, we find

$$\begin{aligned} \Sigma(z) = & \overbrace{G-G} + \overbrace{G-G-G-G} + \overbrace{G-G-G-G-G} \\ & + \overbrace{G-G-G-G-G-G} \\ & + \overbrace{G-G-G-G-G-G-G} \\ & + \overbrace{G-G-G-G-G-G-G-G} \\ & + \overbrace{G-G-G-G-G-G-G-G-G} + \dots, \end{aligned} \quad (\text{B15})$$

where symbol G represents a tunnel vertex, “-” free propagation, and the overlines indicate contraction of lead operators. From this expansion it is clear that the 2vN self-energy contains the set of all diagrams in which there are at most two contraction lines passing over any given point.

4. Counting statistics

Counting fields can easily be added in the kernel Eq. (B14) by replacing the bare tunnel vertices with their gauge-transformed counterparts: $G_1^{p_1} \rightarrow G_1^{p_1} e^{i\xi_1 s_{\alpha_1} p_1 \chi_{\alpha_1}/2}$. The non-Markovian χ -dependent WP self-energy then reads

$$\Sigma(\chi; z) = \mathbf{T}(\chi) \cdot \frac{1}{1 - \mathbf{\Omega} \cdot \mathbf{M}(\chi)} \cdot \mathbf{\Omega} \cdot \mathbf{T}_f(\chi) \quad (\text{B16})$$

with matrices

$$\begin{aligned} T(\chi; 1) &= i\tilde{G}_1^{p_2} e^{i\xi_1 s_{\alpha_1} p_1 \chi_{\alpha_1}/2} \\ T_f(\chi; 1) &= ip_2 f(-\xi_1 p_2 \omega_1) G_1^{p_2} e^{i\xi_1 s_{\alpha_1} p_1 \chi_{\alpha_1}/2} \\ M(\chi; 1, 4) &= \\ & -p_3 f(-\xi_3 p_3 \omega_3) \left\{ \delta_{14} G_3^{p_2} \Omega(1+3) \tilde{G}_3^{p_3} e^{i\xi_3 s_{\alpha_3} (p_3 - p_2) \chi_{\alpha_3}/2} \right. \\ & \left. - \delta_{13} \delta_{42} G_4^{p_2} \Omega(1+4) \tilde{G}_1^{p_3} e^{-i\xi_4 s_{\alpha_4} p_2 \chi_{\alpha_4}/2} e^{i\xi_1 s_{\alpha_1} p_3 \chi_{\alpha_1}/2} \right\} \end{aligned} \quad (\text{B17})$$

where e.g. $\Omega(1+4)$ denotes the free propagator $[z - x_1 - x_4 - \mathcal{L}_D]^{-1}$.

Derivatives of $\Sigma(\chi; z)$ with respect to χ then give the FCS. In the current-block notation of Ref. 34, the stationary current through the system reads

$$\langle I \rangle = \langle\langle \mathcal{J}^{(1)}(\cdot, 0) \rangle\rangle, \quad (\text{B18})$$

and the finite-frequency noise can be written

$$\begin{aligned} S_{\text{qm}}(\omega) = & \langle\langle \frac{1}{2} \mathcal{J}^{(2)}(\cdot, i\omega, 0) + \mathcal{J}^{(1)}(\cdot, i\omega) \Omega_D(i\omega) \mathcal{J}^{(1)}(i\omega, 0) \rangle\rangle \\ & + (\omega \rightarrow -\omega), \end{aligned} \quad (\text{B19})$$

with $\Omega_D(z)$ the effective system propagator and where $\langle\langle \dots \rangle\rangle$ denotes the trace over the stationary state. Writing out explicitly only the sequential and direct-cotunneling contributions, the relevant current blocks read

$$\begin{aligned} \mathcal{J}^{(1)}(z_1, z_0) = & \overbrace{G-X'}_{z_1} + \overbrace{X'-G}_{z_0} \\ & + \overbrace{X'-G-G-G}_{z_0 \ z_0 \ z_0} + \overbrace{G-X'-G-G}_{z_1 \ z_0 \ z_0} \\ & + \overbrace{G-G-X'-G}_{z_1 \ z_1 \ z_0} + \overbrace{G-G-G-X'}_{z_1 \ z_1 \ z_1} + \dots \end{aligned} \quad (\text{B20})$$

$$\begin{aligned} \frac{1}{2!} \mathcal{J}^{(2)}(z_2, z_1, z_0) = & \overbrace{X'-X'}_{z_1} + \frac{1}{2!} \overbrace{X''-G}_{z_0} + \frac{1}{2!} \overbrace{G-X''}_{z_2} \\ & + \overbrace{X'-X'-G-G}_{z_1 \ z_0 \ z_0} + \overbrace{X'-G-X'-G}_{z_1 \ z_1 \ z_0} \\ & + \overbrace{X'-G-G-X'}_{z_1 \ z_1 \ z_1} + \overbrace{G-X'-X'-G}_{z_2 \ z_1 \ z_0} \\ & + \overbrace{G-X'-G-X'}_{z_2 \ z_1 \ z_1} + \overbrace{G-G-X'-X'}_{z_2 \ z_2 \ z_1} \quad (\text{B21}) \\ & + \frac{1}{2!} \overbrace{X''-G-G-G}_{z_0 \ z_0 \ z_0} + \frac{1}{2!} \overbrace{G-X''-G-G}_{z_2 \ z_0 \ z_0} \\ & + \frac{1}{2!} \overbrace{G-G-X''-G}_{z_2 \ z_2 \ z_0} + \frac{1}{2!} \overbrace{G-G-G-X''}_{z_2 \ z_2 \ z_2} + \dots \end{aligned}$$

where X' and X'' represent the first and second derivatives of the χ -dependent tunnel vertex evaluated at $\chi = 0$.

Comparison with Eq. (18) allows us to identify the blocks $\Pi(\omega) = \Omega_D(i\omega)$, $J_{1b}(\omega) = \mathcal{J}^{(1)}(-i\omega, 0)$, $J_{2a}(\omega) =$

$\frac{1}{2}\mathcal{J}^{(2)}(-i\omega, -i\omega, 0)$, and $J_{1a}(\omega) = \mathcal{J}^{(1)}(-i\omega, -i\omega)$ where in the latter two cases, we can throw away all diagrams with a leftmost- G or X'' vertex due to the occurrence of these blocks to the far left in the current and noise expressions.²²

-
- ¹ Y. Blanter and M. Büttiker, *Physics Reports* **336**, 1 (2000).
- ² L. S. Levitov, H. Lee, and G. B. Lesovik, *J. Math. Phys.* **37**, 4845 (1996).
- ³ M. W. Y. Tu and W.-M. Zhang, *Phys. Rev. B* **78**, 235311 (2008).
- ⁴ J. S. Jin, M. T. W. Tu, W. M. Zhang, and Y. J. Yan, *New Journal of Physics* **12**, 083013 (2010).
- ⁵ J. Jin, W.-M. Zhang, X. Q. Li, and Y. J. Yan, “Co-tunneling current noise spectrum through noninteracting systems: An exact n-resolved master equation approach,” (2011), arXiv:1105.0136v1.
- ⁶ J. König, H. Schoeller, and G. Schön, *Phys. Rev. Lett.* **78**, 4482 (1997).
- ⁷ J. König, H. Schoeller, and G. Schön, *Phys. Rev. B* **58**, 7882 (1998).
- ⁸ R. K. Wangsness and F. Bloch, *Phys. Rev.* **89**, 728 (1953).
- ⁹ F. Bloch, *Phys. Rev.* **105**, 1206 (1957).
- ¹⁰ A. G. Redfield, *Adv. Magn. Reson.* **1**, 1 (1965).
- ¹¹ C. Timm, *Phys. Rev. B* **77**, 195416 (2008).
- ¹² S. Koller, M. Grifoni, M. Leijnse, and M. R. Wegewijs, *Phys. Rev. B* **82**, 235307 (2010).
- ¹³ J. N. Pedersen and A. Wacker, *Phys. Rev. B* **72**, 195330 (2005), ;J. N. Pedersen and A. Wacker, *Physica E* **42**, 595 (2010).
- ¹⁴ T. Hansen, V. Mujica, and M. A. Ratner, *Nano Letters* **8**, 3525 (2008).
- ¹⁵ J. Jin, X. Zheng, and Y. Yan, *J. Chem. Phys.* **128**, 234703 (2008).
- ¹⁶ P. Zedler, C. Emary, T. Brandes, and T. Novotný, *Phys. Rev. B* **84**, 233303 (2011).
- ¹⁷ When we refer to the order of a method, we refer to the power of Γ , and not that of the tunneling elements.
- ¹⁸ H. A. Nilsson, O. Karlström, M. Larsson, P. Caroff, J. N. Pedersen, L. Samuelson, A. Wacker, L.-E. Wernersson, and H. Q. Xu, *Phys. Rev. Lett.* **104**, 186804 (2010).
- ¹⁹ O. Karlström, J. N. Pedersen, P. Samuelsson, and A. Wacker, *Phys. Rev. B* **83**, 205412 (2011).
- ²⁰ A. O. Gogolin and A. Komnik, *Phys. Rev. B* **73**, 195301 (2006).
- ²¹ J. König, J. Schmid, H. Schoeller, and G. Schön, *Phys. Rev. B* **54**, 16820 (1996).
- ²² C. Emary, *Journal of Physics: Condensed Matter* **23**, 025304 (2011).
- ²³ M. Braun, J. König, and J. Martinek, *Phys. Rev. B* **74**, 075328 (2006).
- ²⁴ P. Zedler, *Master equations in transport statistics*, Ph.D. thesis, Technische Universität Berlin (2011).
- ²⁵ A. Braggio, J. König, and R. Fazio, *Phys. Rev. Lett.* **96**, 026805 (2006).
- ²⁶ V. Kashcheyevs, A. Schiller, A. Aharony, and O. Entin-Wohlman, *Phys. Rev. B* **75**, 115313 (2007).
- ²⁷ V. Meden and F. Marquardt, *Phys. Rev. Lett.* **96**, 146801 (2006).
- ²⁸ H.-W. Lee and S. Kim, *Phys. Rev. Lett.* **98**, 186805 (2007).
- ²⁹ A. Silva, Y. Oreg, and Y. Gefen, *Phys. Rev. B* **66**, 195316 (2002).
- ³⁰ P. G. Silvestrov and Y. Imry, *Phys. Rev. B* **75**, 115335 (2007).
- ³¹ A. Carmi and Y. Oreg, *Phys. Rev. B* **85**, 045325 (2012).
- ³² M. Leijnse and M. R. Wegewijs, *Phys. Rev. B* **78**, 235424 (2008).
- ³³ H. Schoeller, *The European Physical Journal - Special Topics* **168**, 179 (2009).
- ³⁴ C. Emary and R. Aguado, *Phys. Rev. B* **84**, 085425 (2011).